Multispectral remote sensing of landscape level foliar moisture: techniques and applications for forest ecosystem monitoring

Michael Toomey and Lee A. Vierling

Abstract: Broad-scale monitoring of varying moisture levels of leaves has ramifications for understanding fire potential, biogeochemistry, and ecosystem dynamics. Five different shortwave infrared (SWIR)-derived spectral indices, principal components analysis (PCA), and the tasseled cap transformation (TCT), derived from Landsat Thematic Mapper (TM) and Advanced Spaceborne Thermal Emission and Reflection Radiometer (ASTER) satellite data, were used to quantify landscape-level foliar moisture in an ecosystem dominated by *Pinus ponderosa* P. & C. Lawson. Landsat TM data demonstrated stronger correlations with in situ calculations of foliar moisture than did ASTER data. The second principal component correlated strongly with ground data (r^2 = 0.765). The Landsat-derived TCT wetness component was significantly correlated with ground data (r^2 = 0.638) as well as a normalized difference NIR/SWIR ratio (r^2 = 0.834). The spectral indices and TCT are more practical for ecosystem moisture monitoring than PCA because of the empirical nature of PCA. Based on these results, we recommend modifications to existing methods of satellite-based fire susceptibility monitoring to account for primary effects of vegetation curing and temporal variation in ground fuels.

Résumé : La détection à grande échelle des variations de teneur en eau des feuilles peut être utile pour comprendre le potentiel calorifique, la biogéochimie et la dynamique des écosystèmes. Cinq indices spectraux différents, dérivés de l'infrarouge ondes courtes (IROC), l'analyse en composante principale (ACP), l'espace indiciel transformé (TCT) dérivé des données satellitaires du capteur TM de Landsat (TM) et du radiomètre spatiale de pointe pour l'étude de la réflectance et des émissions thermiques terrestres (ASTER) ont été utilisés pour quantifier la teneur en eau des feuilles à l'échelle du paysage dans un écosystème dominé par *Pinus ponderosa* P. & C. Lawson. Les données de Landsat TM sont plus étroitement corrélées aux calculs in situ de la teneur en eau des feuilles que celles d'ASTER. La deuxième composante principale est fortement corrélée avec les données de terrain r^2 = 0,765. La composante de TCT pour la teneur en eau dérivée des données de Landsat est significativement corrélée aux données de terrain (r^2 = 0,638) aussi bien qu'un rapport (PIR/IROC) de différences normalisées (r^2 = 0,834). Les indices spectraux et le TCT sont plus pratiques pour le suivi de la teneur en eau des écosystèmes que l'ACP étant donné la nature empirique de l'ACP. Sur la base de ces résultats, nous recommandons des modifications aux méthodes existantes de télédétection des risques de feu pour tenir compte des effets primaires du dessèchement de la végétation et des variations temporelles dans les combustibles au sol.

[Traduit par la Rédaction]

Introduction

Monitoring the varying moisture levels of leaves has ramifications for understanding fire potential, plant stress, biogeochemistry, and ecosystem dynamics. Studies of the spectral response to changes in plant water content have been conducted for several decades (e.g., Gates et al. 1965; Al Abbas et al. 1974; Carter 1991), but the majority of this work has been conducted in the laboratory. Despite the advances within this area of study, broadband remote sensing of landscape-level foliar moisture in conifers is still relatively unexplored. The shortwave infrared (SWIR) region (1400–2500 nm) exhibits low to moderate reflectance (15%–30%) by leaves, is strongly correlated with leaf water content (Woolley 1971; Gausman 1973; Tucker 1980), and is gaining attention for use in vegetation studies (Cohen and Goward 2004). Incorporation of SWIR bands has yielded accurate estimates of LAI and biomass (Gao 1996; Chen et al. 2002), stand age (Steininger 2000), fire potential (Maki et al. 2004), and canopy chemistry (Wessman et al. 1988). Sensitivity to water content of foliage is most pronounced in the SWIR (Fig. 1).

A common parameter for assessing fire potential is the foliar moisture content (FMC), as defined by

$$[1] \qquad \mathrm{FMC} = \frac{M_{\mathrm{Fresh}} - M_{\mathrm{Dry}}}{M_{\mathrm{Dry}}} \times 100\%$$

where M is the mass of fresh and dry leaves. At the canopy level, the site moisture concentration (SMC) describes the total mass of water in the canopy and understory per unit

Received 26 August 2004. Accepted 24 January 2005. Published on the NRC Research Press Web site at http://cjfr.nrc.ca on 21 May 2005.

M. Toomey and L.A. Vierling.[1,2] Institute of Atmospheric Sciences, South Dakota School of Mines and Technology, 501 East Saint Joseph Street, Rapid City, SD 57701, USA.

[1]Corresponding author (e-mail: leev@uidaho.edu).
[2]Present address: College of Natural Resources, University of Idaho, Moscow, ID 83844, USA.

 doi: 10.1139/X05-043

Fig. 1. Spectral reflectance of fresh (107% foliar moisture content (FMC)) and dry (78% FMC) *Pinus ponderosa* needles.

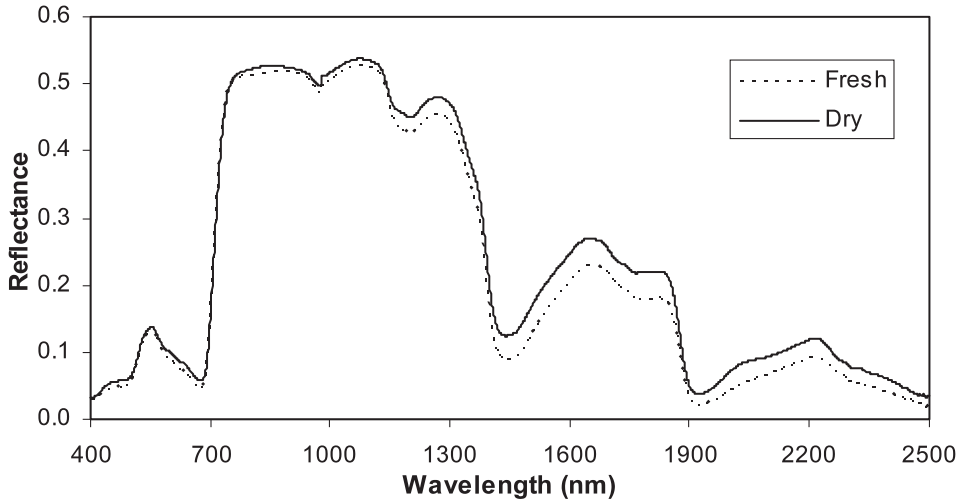

area of land (kilograms per square metre). SMC is comparable to the equivalent water thickness (EWT), which describes a theoretical layer of water with uniform depth (reported as centimetres of water or kilograms per square metre) that would produce an observed spectral response (Roberts et al. 1997).

Several laboratory studies have found a strong correlation between the water content of leaves and SWIR reflectance. Carter (1991) hydrated leaves to full turgor and allowed them to dry, collecting the spectra at the ensuing levels of dessication. SWIR reflectance of the evergreen *Magnolia grandiflora* increased five-fold with dessication. Recently, Sims and Gamon (2003) found that the 1520–1540 nm region was optimal for detecting moisture content variations in 23 different annual, vine, shrub, deciduous, and evergreen tree species from the Sierra Nevada.

A number of studies have been conducted to remotely sense canopy-scale moisture levels. Hardy and Burgan (1999) found that a time series of NDVI was sensitive to grass and forest understory foliar moisture, but not to that of shrubs or coniferous forest canopies. Peñuelas et al. (1993) successfully used a ρ970/ρ900 index (where ρ is reflectance and the number is the central wavelength of the band, in nanometres) to detect water content variations in potted plants. In California chaparral, Serrano et al. (2000) encountered significant correlation between foliar water content and the narrow-band indices normalized difference infrared index (NDII; Hardisky et al. 1983) and normalized difference water index (NDWI; Gao 1996):

$$[2] \qquad \mathrm{NDII} = \frac{(\rho_{819} - \rho_{1649})}{(\rho_{819} + \rho_{1649})}$$

$$[3] \qquad \mathrm{NDWI} = \frac{(\rho_{857} - \rho_{1241})}{(\rho_{857} + \rho_{1241})}$$

Chuvieco et al. (1999) also found NDII to be a very accurate indicator of FMC in Mediterranean grass and shrublands ($r^2 \approx 0.9$). Incorporating a 1241-nm water absorption band, NDWI has also shown strong correlation with FMC in *Pinus edulis* in the laboratory ($r^2 = 0.91$; Stimson et al. 2003). NDWI has demonstrated strong potential for estimating canopy water content with canopy reflectance models of jack pine stands (Dawson et al. 1999) and with Moderate Resolution Imaging Spectrometer (MODIS; Dennison et al. 2003) and Advanced Visible Infrared Imaging Spectrometer (AVIRIS) data in California chaparral (Serrano et al. 2000). AVIRIS also facilitates differentiation of surface liquid water content from atmospheric water vapor due to a 20-nm gap between liquid and vapor absorption peaks in the near infrared (NIR) and is thus useful for deriving EWT (Roberts et al. 1997). This procedure entails deriving the slope from a linear model of the natural log of reflectance in the 867–1088 nm region for each pixel.

Jacquemoud et al. (1995) modeled reflectances of sugar beet canopies to estimate EWT with simulated multi- and hyper-spectral platforms, deriving accurate estimations with an average RMSE of reflectance of 3.2% and 3.7% for TM and AVIRIS, respectively. Ceccato et al. (2002*b*) compared the EWT of four xeric and mesic landscapes with their model-derived global vegetation monitoring index (GVMI; Ceccato et al. 2002*a*):

$$[4] \qquad \mathrm{GVMI} = \frac{(\rho_{\mathrm{NIR}} + 0.1) - (\rho_{\mathrm{SWIR}} + 0.2)}{(\rho_{\mathrm{NIR}} + 0.1) + (\rho_{\mathrm{SWIR}} + 0.2)}$$

finding strong correlations ($r^2 = 0.93$).

With the exception of Jacquemoud et al. (1995) and Ceccato et al. (2002*b*), the methods of the aforementioned studies require access to hyperspectral sensors. Of them, only the work of Dawson et al. (1999) has produced successful results with coniferous stands. Because of high cost and limited availability, such methods are not practical at this time for extended monitoring of forests and other ecosystems. Further, the multispectral work by Jacquemoud et al. (1995) and Ceccato et al. (2002*b*) require model inversion and considerable in situ biochemical and biophysical data, which may be untenable for some users working with large heterogeneous forest tracts. The intent of this study is to develop methodologies for monitoring site moisture that could be implemented inexpensively and regularly with the many SWIR-capable multispectral remote sensing platforms available today. Recently, Dennison et al. (2004) and Stow et al. (2004) used indices derived from MODIS to estimate

changes in live fuel moisture. In this paper, multiple combinations of wide-band indices, principal components analysis (PCA), and tasseled cap transformation (TCT) are used to determine the most viable scheme for assessing SMC in Ponderosa pine (*Pinus ponderosa* P. & C. Lawson) ecosystems, using Landsat TM and ASTER imagery. We hypothesize that ASTER, with its greater SWIR spectral resolution and signal-to-noise ratios, should yield more accurate estimations of SMC. ASTER, designed largely for geological remote sensing, has not been used widely for vegetation studies, and such potential warrants study.

Materials and methods

SWIR moisture indices

While SWIR reflectance is primarily associated with water absorption, its reflectance alone cannot be used to estimate landscape-level moisture content. Ceccato et al. (2001) discovered that secondary factors such as internal structure and dry matter influence SWIR reflectance at the leaf level. The effects propagate to the landscape level (Ceccato et al. 2002*b*). In addition, certain backgrounds can even reverse the expected SWIR–water relationship in stacked leaves (Lillesaeter 1982), whereby SWIR reflectance may increase with added leaf layers. Therefore, to estimate foliar moisture content in a variety of ecosystems, one must account for the contrasting spectral characteristics of leaves and the water that they contain. The former may be quantified with a vegetation index comprising visible and NIR bands, and the latter with the SWIR bands.

A multitude of vegetation indices are available for the quantification of leaf density, and three of the most commonly used indices are incorporated here: the simple ratio (SR; Birth and McVey 1968), the normalized difference vegetation index (NDVI; Rouse et al. 1974), and the enhanced vegetation index (EVI; Huete et al. 1997). SR and NDVI have been used extensively for arboreal remote sensing, often exhibiting accurate LAI estimations in coniferous forests (Spanner et al. 1994; Wulder et al. 1998; Chen et al. 2002). NDVI can be insensitive to biomass and LAI in dense forests (Sellers 1985; Hall et al. 1995; Roberts et al. 2004), which is not problematic in our study area, considering the low LAI values found there. EVI was specifically designed to quell atmospheric effects and background contamination (Huete et al. 1997) and demonstrates superiority over SR and NDVI for vegetation density estimation (Gao et al. 2000) and vegetation detection under smoky skies (Miura et al. 2001). To estimate foliar moisture, we create three simple moisture indices, dubbed MI1 (moisture index 1), MI2, and MI3, by dividing the three vegetation indices by the SWIR band reflectance. These indices contrast the cellular and moisture-related spectral properties of the canopy, ensuring that SWIR reflectance variations are not due solely to biomass changes:

$$\mathrm{MI1} = \frac{\rho\mathrm{NIR}}{\rho\mathrm{RED} \times \rho\mathrm{SWIR}}$$

$$\mathrm{MI2} = \frac{(\rho\mathrm{NIR} - \rho\mathrm{RED})}{(\rho\mathrm{NIR} + \rho\mathrm{RED}) \times \rho\mathrm{SWIR}}$$

$$\mathrm{MI3} = \frac{2.5 \times (\rho\mathrm{NIR} - \rho\mathrm{RED})}{(1 + \rho\mathrm{NIR} + 6 \times \rho\mathrm{RED} - 7.5 \times \rho\mathrm{BLUE}) \times \rho\mathrm{SWIR}}$$

Inclusion of the visible bands introduces another major factor of leaf reflectance: chlorophyll content. Foliar water loss typically induces a decrease in chlorophyll concentrations (Carter 1991; Burgan et al. 1996). Red band reflectance may aid moisture variation detection in some cases. In the case of MI1, for instance, moisture loss would effect a simultaneous increase of red and SWIR reflectance, enhancing the sensitivity of the index to water content. Moisture and chlorophyll concentrations, however, do not always vary in tandem (Larcher 1995). Consequently, two NIR- and SWIR-derived indices, the infrared ratio (IR) and NDII, which exclude the chlorophyll-sensitive visible bands, are also used in this study:

$$\mathrm{IR} = \frac{\rho\mathrm{NIR}}{\rho\mathrm{SWIR}}$$

$$\mathrm{NDII} = \frac{(\rho\mathrm{NIR} - \rho\mathrm{SWIR})}{(\rho\mathrm{NIR} + \rho\mathrm{SWIR})}$$

The two indices demonstrate close correlations with water variations at the leaf (Ceccato et al. 2001) and canopy scale (Ceccato et al. 2002*b*), respectively. Values of all five indices are expected to rise with increasing foliar moisture, predominantly because of the increase in NIR reflectance and decrease in SWIR reflectance.

Two image transformations were also implemented in this study: PCA and TCT wetness component. PCA reduces the dimensionality of multispectral and hyperspectral imagery into fewer vectors that explain the majority of variation in the data (see Schowengerdt 1997 for further reading). Each vector is a set of coefficients, referred to as eigenvectors, which are applied to each band to produce a scalar quantity for each pixel. PCA was performed on forested subsets of both the Landsat and ASTER images. The TCT, which is mathematically similar to the PCA but is data independent (Crist et al. 1986), was performed on all Landsat images. TCT wetness has been implemented successfully for detecting moisture variations associated with forest mortality (Collins and Woodcock 1996; Skakun et al. 2003).

Site characteristics

The study area is located in the north-central Black Hills of South Dakota (44°10′N, 103°37′W), within and proximal to the Black Hills Experimental Forest (BHEF). Fifty-one plots were distributed throughout a 30-km^2 area at 10 closely spaced subsites. Each of the 25 m × 25 m plots was selected for level terrain (slope less than 12°) and homogeneous canopy, and located with differentially corrected global positioning systems (GPS). The combination of varied harvesting and topography yields the juxtaposition of a wide gamut of canopy types in the BHEF. Immature, semimature, mature, and old-growth stands, with variable understory cover, are all found interspersed throughout the region, allowing a wide spectrum of moisture levels and overstory–understory relationships to be represented. The overstory is largely dominated by *P. ponderosa* and contains small stands of white

spruce (*Picea glauca*) and aspen (*Populus tremuloides*) on north-facing slopes. The understory of the drier sites is dominated by bearberry (*Arctostaphylos uva-ursi*), wheatgrass (*Pascopyrum smithii*), and common juniper (*Juniperus communis*), while many of the moist north-facing slopes are dominated by rough-leaved ricegrass (*Oryzopsis asperifolia*), common juniper, and numerous forbs.

Ecological measurements

Ecological measurements were conducted between 13 July and 8 August 2003. The in situ information was compared with the most recent Landsat (±8 days) or ASTER (±8 days) image, to minimize errors due to daily moisture variation. Additionally, collections were performed within a 2-h window about the time of the satellite overpass to recreate the solar conditions. Minor precipitation fell on 26 and 27 July, during which time no collections were made, and on 8 August, several hours before the collection (USGS 2003; Fig. 2). On the latter date, samples were surface-dried to ensure accurate FMC values. Site moisture concentration (SMC) was used to quantify canopy water content as the total leaf moisture per unit area (kilograms H_2O per square metre). Equation 7 shows the derivation of SMC.

SMC was estimated for the overstory and understory by dissimilar methodologies. The former was calculated using a combination of optical methods and direct moisture measurements. To assess the SMC of the overstory, the foliar moisture content (eq. 2) and total mass of foliage must be determined. FMC was measured in the field by extracting a dozen needle samples (>2.00 g per sample) at three different canopy levels: the uppermost 2 m, the lower 2 m, and mid-canopy. Fresh mass was measured in the field with a portable balance (0.01-g accuracy). Afterward, the samples were dessicated for at least 24 h at 80 °C.

Total mass of overstory foliage was determined indirectly by assessment of the leaf area index (LAI), a unitless (metres squared per metre squared) measure of half the total leaf area per unit area of ground. LAI is calculated as follows (Chen 1996):

$$[5] \qquad \mathrm{LAI} = \mathrm{LAI_e}(1-\alpha)\frac{\gamma_E}{\Omega_E}$$

where $\mathrm{LAI_e}$ is the effective LAI, α is the woody to total area ratio, γ_E is the clumping of needles around the shoot (i.e., the needle to shoot area ratio), and Ω_E is the clumping at levels larger than the shoot. Values for γ_E and α were adopted from the work of Law et al. (2001) and are given as 1.25 and 0.27, respectively. We estimated Ω_E with the Tracing Radiation and Architecture of Canopies (TRAC; 3rd Wave Engineering, Nepean, Ontario, Canada) instrument. TRAC measures variations in the photosynthetic photon flux density (PPFD) to quantify the clumping of shoots, branches, and trees. $\mathrm{LAI_e}$ was measured using the LAI-2000 instrument (Li-COR, Inc., Lincoln, Nebraska, USA). Six LAI-2000 measurements and two 25-m TRAC transects were made per plot. LAI of the plot was divided by the specific leaf area (SLA, the half surface area of 1 g of foliage), to determine the mass of foliage per unit area (MFA; kilograms per square metre). The SLA assumed for *P. ponderosa* is 43.8 $\mathrm{cm^2/g}$ (Law et al. 2001).

Understory moisture concentrations were determined directly by means of destructive measurements. Within each plot, four 0.25-$\mathrm{m^2}$ quadrats were placed at designated locations, and all photosynthetic tissue inside the quadrat was removed. The mass of the understory vegetation at each location was measured with a portable balance. Samples were returned to the lab and dessicated at 80 °C for at least 24 h. The understory moisture concentration per unit area (UMA; kilograms per square metre) for each plot was calculated as

$$[6] \qquad \mathrm{UMA} = \sum_{i=1}^{n=4} M_{\mathrm{Fresh}} - M_{\mathrm{Dry}}$$

where n is the number of quadrats per plot. Because it is very time consuming to remove all the needles from the *J. communis* plant within a quadrat, their site moisture concentration was determined by volumetric inventory, which we define as grams of needles per cubic metre of juniper. Volumetric inventory was determined with destructive measurements, assuming a semicylindrical shape. At each plot, the volumetric distribution of juniper was measured, and juniper FMC was measured separately from the other understory vegetation. These samples were dried to the previously mentioned specifications to determine the juniper moisture content per unit area (JMA). The percentage of area covered by juniper ($\%A_J$) versus all other vegetation ($\%A_U$; the sum of the two always equals 100%) was estimated from the volumetric juniper measurements. SMC was determined by incorporating these data into the following equation:

$$[7] \qquad \mathrm{SMC} = \mathrm{MFA_o} \times \mathrm{FMC_o} + (\%A_U \times \mathrm{UMA} + \%A_J \times \mathrm{JMA})$$

where the o subscript denotes values for the *P. ponderosa* overstory.

Landsat and ASTER image acquisition and processing

Three Landsat 5 images were used for comparison with the ecological measurements in this study: 13 July, 20 July, and 5 August 2003. The images were radiometrically corrected, georectified using ground control points (cubic convolution resampling; RMSE = 0.7 pixels), and corrected for topographically induced parallax error by the EROS Data Center (Sioux Falls, South Dakota). Atmospheric corrections were performed by means of a dark object subtraction (Chavez 1988). Image-to-image radiometric normalization was explored but not performed because of the fact that very few nonvegetated pixels are present in the area, and analyses using these pseudoinvariant features indicated that potential normalization errors were on the order of 1%–3% in the relevant bands. Landsat has two SWIR bands available for calculating indices, TM5 (1550–1750 nm) and TM7 (2080–2035 nm). Overlays of the GPS-located plots were used to identify the corresponding pixel in the image.

Two images of ASTER level 7 surface reflectance data were also incorporated from 21 July and 6 August 2003. The surface reflectance product is generated by the ASTER Ground Data System from a level 1B radiometrically, geometrically, and parallax-corrected radiance product. The 1B product is atmospherically corrected using assumed optical thickness and exogenous aerosol parameters (Thome et al.

Fig. 2. Daily precipitation, maximum temperature, and dates of ecological measurements and satellite overpasses. Meteorological data courtesy of USGS (2003). Note the light precipitation on 8 August. This rain fell hours before data collection, and all samples were surface-dried before weighing.

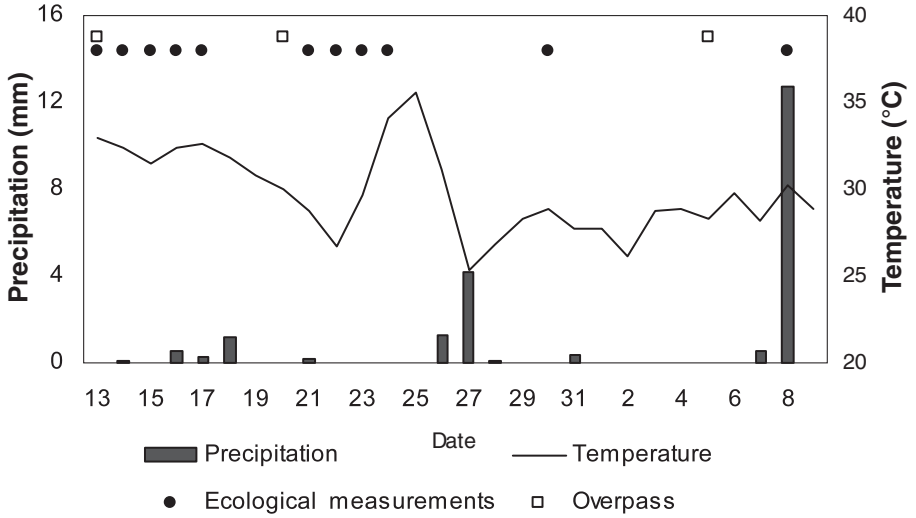

1999) to produce the level 7 image. The 30-m SWIR band images were resampled to match the 15-m resolution of the visible and NIR band images. GPS-located plot overlays were used to identify the corresponding 2 × 2 pixel subsets. The images were georectified in ENVI 4.0, using 30 ground control points from a USGS digital orthophoto quadrangle.

Four ASTER SWIR bands were used in this study: band 4 (1600–1700 nm), band 6 (2185–2225 nm), band 7 (2235–2285 nm), and band 8 (2295–2365 nm). Bands 5 and 9 were excluded from the study because of a phenomenon known as "crosstalk", where neighboring SWIR detectors are susceptible to photons reflected off of the band 4 detector. The effect is strongest in bands 5 and 9, since their detectors are physically closest to that of band 4 (ERSDAC 2002). This effect is noticeable primarily in highly reflective urban settings and dark–bright interfaces such as water and land boundaries. Neither situation pertains to the homogeneous forested landscape that is being studied. Software is being developed by other researchers to ameliorate this effect, but it was not available for this investigation.

The high NIR reflectance of leaves tends to accelerate the increase of vegetation indices when LAI is increased from 0 to 3, producing a nonlinear relationship between indices and biophysical parameters (Sellers et al. 1985; Chen et al. 2002). Hence, logarithmic and exponential statistical models were used to compare satellite measurements and field-measured SMC. Results are reported as the coefficient of determination (r^2) and represent the best-fit nonlinear model.

Results and discussion

Ecological measurements

LAI values for the 51 plots ranged from 0.49 to 2.99, with an average LAI of 1.68 (Table 1). The average FMC of the overstory was 108.6%; the standard deviation of 10.6% indicates the small range in moisture values. Typically, FMC of the lower 2 m of the canopy was higher than that of the upper 2 m of the canopy by 15%–20%. Overstory moisture content was almost six times as great as understory moisture, on average. Several plots with dense overstory canopies had little understory vegetation and vice versa. Nonetheless, even in medium-density canopies, there was a fairly continuous vegetative cover, because dense understory growth occurs below gaps in the overstory. The mean SMC was 0.468 kg H_2O/m^2 and ranged from 0.181 kg H_2O/m^2 in some of the heavily managed zones to 0.819 kg H_2O/m^2 in the north-facing, mature, and old-growth stands (Table 1). These values are similar to those estimated for boreal jack pine stands (Dawson et al. 1999).

SWIR moisture indices

There is a strong correlation between TM5 and TM7 SWIR bands for forested pixels (r^2 = 0.918), with TM7 reflectance approximately half that of TM5. Consequently, subsequent analyses were performed solely with TM5, since TM5 retains slightly more sensitivity in this high-moisture range. All regression analyses produced significant relationships ($p < 0.001$). There is little difference in the performance of the various Landsat band combinations. Of the three moisture indices, MI3 has the strongest correlation with SMC (r^2 = 0.576; Table 2). MI3 incorporates EVI, which has demonstrated superior detection of understory and overstory vegetation on a global scale (Huete et al. 2002). Very similar agreement was encountered with IR (r^2 = 0.576), and fewer outliers exist with IR. The strongest correlation overall was with NDII (r^2 = 0.584), which exhibited a strongly curvilinear relationship with the in situ data. Ceccato et al. (2002*b*), using a global sensitivity analysis of modeled reflectances, established that NIR and SWIR are the required bands for canopy foliar moisture estimation.

To determine whether simple vegetation indices may be used as a proxy for SMC estimation, regression of SR, NDVI, and EVI (without the SWIR band) with SMC was performed. The weaker correlation (r^2 = 0.360, 0.376, and 0.137, respectively) underscores the importance of SWIR in estimating foliar moisture. To determine the relative importance of NIR and SWIR in estimating SMC, a number of weighting schemes were applied to the most successful index, NDII (data not

Table 1. Summary of leaf area index (LAI) and moisture measurements.

	Effective LAI	TRAC (Ω)*	Overstory LAI (m^2/m^2)	FMC (%)†	Overstory moisture (kg/m^2)	Understory moisture (kg/m^2)	SMC‡ (kg/m^2)
Avg.	1.558	0.836	1.68	108.6	0.417	0.069	0.486
Min.	0.450	0.545	0.49	90.5	0.114	0.004	0.181
Max.	2.660	1.000	2.99	134.0	0.725	0.161	0.819
SD	0.611	0.097	0.59	10.6	0.152	0.039	0.144

*Clumping factor as determined by Tracing Radiation and Architecture of Canopies (TRAC).
†Foliar moisture concentration.
‡Total site moisture concentration for an entire plot, calculated independently of the previous two columns.

Table 2. Coefficients of determination (r^2; $p < 0.001$) and best-fit regression equations of various Landsat indices and image transformations to site moisture concentration.

	r^2	Best-fit equation
MI1	0.521	$y = 96.141x^{1.003}$
MI2	0.552	$y = 10.459x^{0.759}$
MI3	0.576	$y = 4.276x^{0.753}$
IR	0.576	$y = 0.759\ln x + 2.051$
NDII	0.584	$y = 0.289\ln x + 0.395$
wNDII	0.627	$y = 0.734x^{0.605}$
PC1	0.683	$y = -0.081\ln x - 0.093$
PC2	0.765	$y = 0.056\ln x + 0.035$
TCTwet	0.638	$y = 25.197\ln x - 1.795$

Note: MI1, MI2, and MI3, moisture index 1, 2, and 3, respectively; IR, infrared ratio; NDII, normalized difference infrared index (see Materials and methods for index formulas); PC1 and PC2, first and second principal components; TCTwet, tasseled cap transformation wetness component. In the equations, the index is the dependent variable and SMC is the independent variable.

shown). The NIR and SWIR bands were weighted separately from 1 to 5 in increments of 0.5. Weighting the NIR reflectance by a factor of two optimized the NDII–SMC relationship ($r^2 = 0.627$; Fig. 3*a*):

$$[8] \qquad \text{wNDII} = \frac{2\rho_{NIR} - \rho_{SWIR}}{2\rho_{NIR} + \rho_{SWIR}}$$

where wNDII is weighted NDII. Heavier weighting of the NIR band yielded no significant improvements in the correlation, but narrowed the range of index values. Weighting the SWIR reflectance made no significant improvements.

The wNDII–SMC relationship was further strengthened by the exclusion of 16 plots. Seven of these plots had dense understories of rough-leaved ricegrass (*O. asperifolia*) cover. It is widely recognized that NIR scattering by broadleaves is far greater than with needleleaves (Spanner et al. 1990; Chen et al. 2002). Therefore, plots with ample cover of rough-leaved ricegrass exhibit high NIR reflectance, leading to anomalously high NDII values. Their omission from the regression increased the r^2 value to 0.668. Further, the thin epidermis of the grass allows for greater penetration and absorption of SWIR (Sims and Gamon 2003) than does the thick sheath of pine needles. In addition, nine plots were excluded that were originally compared to imagery taken 16 days later, because of cloud cover during earlier satellite overpasses. With the more refined data set, the correlation strengthened considerably ($r^2 = 0.834$; Fig. 3*b*). These results underscore the importance of temporal comparability of ground and satellite data.

Fig. 3. Landsat TM weighted normalized difference infrared index (wNDII) versus site moisture concentration (SMC) ($p < 0.001$) with (*a*) all plots and (*b*) excluding plots with dense *Oryzopsis asperifolia* cover. In (*a*) squares represent plots with dense *O. asperifolia* and triangles represent plots bearing a 16-day discrepancy between ecological measurements and satellite measurements.

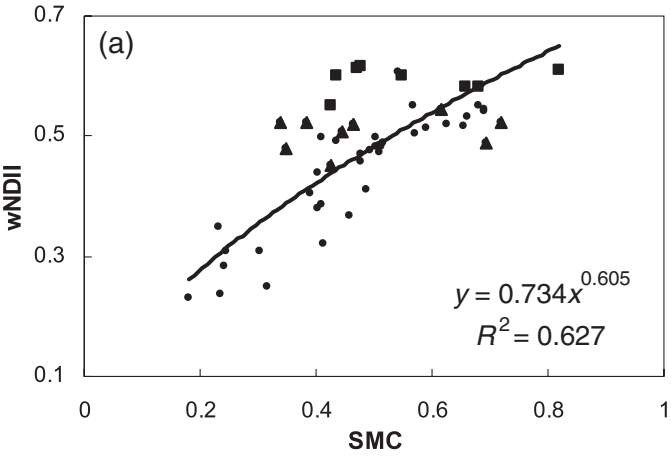

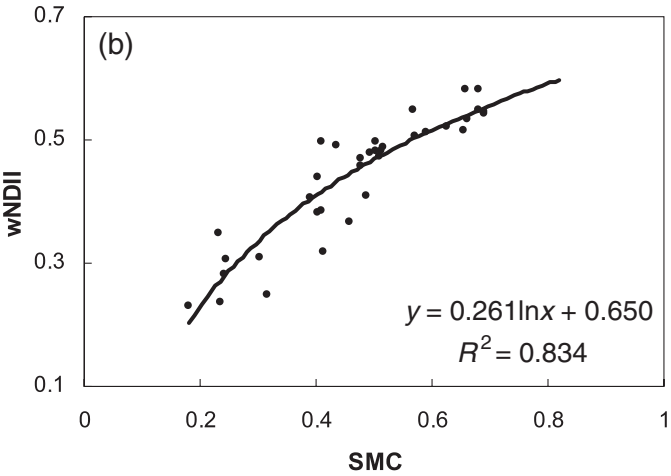

All of the aforementioned indices were calculated with the ASTER data, save the EVI, because of the absence of a

blue band. To fully explore the SMC prediction potential of ASTER, index values were calculated for each SWIR band (4, 6–8) individually. Overall, ASTER performed more poorly than Landsat, exhibiting lower r^2 values with SMC than Landsat, ranging from 0.42 to 0.53 (Table 3). MI2 exhibited the strongest correlations with SMC ($r^2 = 0.549$), with slightly higher coefficients of determination than with NDII and wNDII. For each index, the strongest correlation was encountered with band 4, the near equivalent of TM5. Nonetheless, there seems to be a benefit to including the red band for SMC estimation with ASTER.

Table 3. Best-fit regression coefficients (r^2; $p < 0.001$) between ASTER (AS) indices and site moisture concentration (SMC).

	AS4	AS6	AS7	AS8
MI1	0.506	0.470	0.483	0.469
MI2	0.549	0.491	0.508	0.487
IR	0.474	0.424	0.426	0.435
NDII	0.511	0.486	0.473	0.509
wNDII	0.512	0.465	0.479	0.470

Note: Rows indicate the index used and columns indicate the SWIR band incorporated. MI1, MI2 and MI3 are moisture index 1, 2, and 3, respectively; IR, infrared ratio; NDII, normalized difference infrared index (see Materials and methods for index formulas).

Image transformations

PCA is data dependent and therefore is best used to analyze single images. Consequently, PCA was performed on one image in which SMC values were adjusted for temporal variations. Temporal changes in moisture were assessed by first calculating weighted NDII (wNDII) values for all plot locations using the 5 August image, and then comparing the results with the wNDII values from the image that was acquired closest in time to the ground SMC collection. SMC values were amended by using the reverse form of the wNDII–SMC regression function, with a correction for moisture loss during the period.

For example, for plots surveyed for the 13 July image, using the regression function (Fig. 3*a*)

$$[9] \qquad \text{wNDII} = 0.734\text{SMC}^{0.605}$$

and compensating for a 6.12% reduction in NDII (93.9% of original wNDII) between the 13 July and 5 August scene, the time-adjusted SMC for 5 August is given by

$$[10] \qquad \left(\frac{0.939\text{wNDII}}{0.734}\right)^{1.653} = \text{SMC}$$

The use of the multiplier (0.939 in eq. 10) to wNDII retains natural variation and range of estimated SMC values between plots.

The correlation between SMC and the first principal component (PC1) was quite strong ($r^2 = 0.683$; Table 2) and exhibited a negative curvilinear relationship. A stronger positive relationship with PC2 ($r^2 = 0.765$; Fig. 4*a*) was found. PC2 of Landsat imagery is commonly associated with vegetation characteristics. Hence, it is not surprising that the most significant correlation between satellite and in situ data is established by the second PC. TCT wetness was also applied to the image and demonstrated a slightly higher correlation with SMC ($r^2 = 0.638$; Fig. 4*b*) than was found with wNDII. The strong correlation with SMC is attributed to the heavy weighting of the SWIR bands.

PCA was also performed on the ASTER images. Because all but three plots are within 9 days of the 21 July image, PCA was performed on the 21 July image for the remaining 48 plots. Coefficients of determination between first, second, and third PCs are 0.468, 0.517, and 0.490, respectively. Similar to results with Landsat, the second PC provided the strongest correlation with field data.

Eigenvector coefficients for Landsat and ASTER exhibit a similar direction and magnitude in PC1, where all bands are positive (Table 4), indicating that PC1 is related to general brightness. It is noteworthy that the PC2 eigenvector coefficients are positive only with NIR for both TM and ASTER. In comparison, the TCT wetness coefficients are positive for both the visible and the NIR bands (Table 4A), yet SMC has an inverse relationship with both visible (data not shown) and SWIR bands. This may be why PC2, with negative coefficients for all absorption bands, exhibits higher correlation with in situ data than do ASTER PC3 and TCT wetness.

Fig. 4. (*a*) Landsat TM second principal component (PC2) and (*b*) tasseled cap transformation (TCT) wetness component versus site moisture concentration (SMC) ($p < 0.001$).

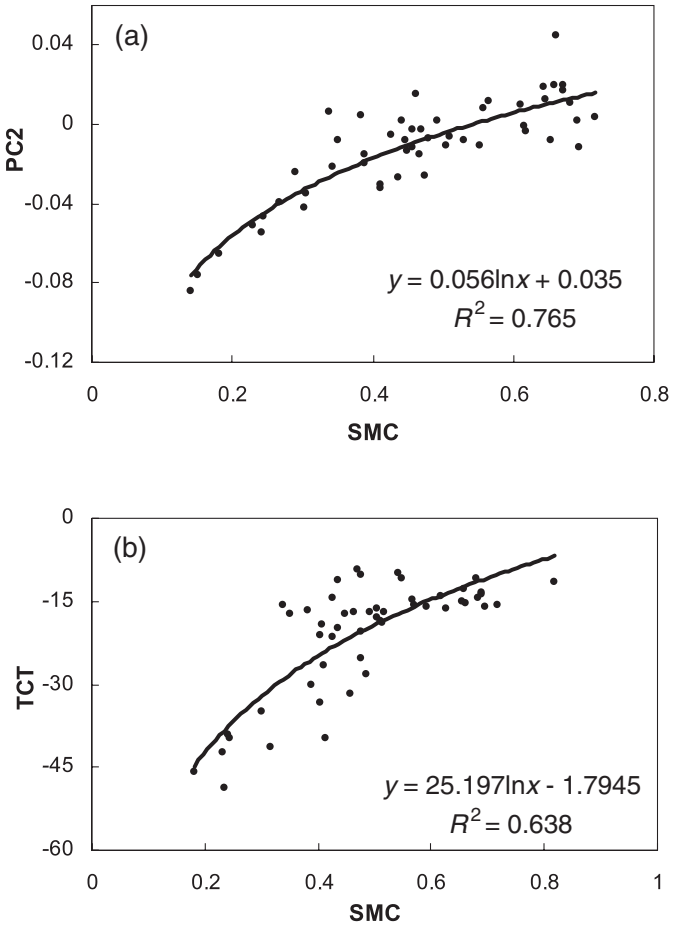

Table 4. Eigenvector coefficients for (A) Landsat (TM) and (B) ASTER (AS) image transformations.

(A) Eigenvector coefficients for Landsat.						
	TM1	TM2	TM3	TM4	TM5	TM7
PC1	0.0830	0.1420	0.1819	0.5912	0.6606	0.3924
PC2	–0.0881	–0.0938	–0.2058	0.7924	–0.3741	–0.4161
TCT	0.1446	0.1761	0.3322	0.3396	–0.6210	–0.4186

(B) Eigenvector coefficients for ASTER.							
	AS1	AS2	AS3	AS4	AS6	AS7	AS8
PC1	0.1771	0.1561	0.7428	0.4823	0.2532	0.2204	0.2173
PC2	–0.1568	–0.2598	0.6499	–0.3705	–0.3727	–0.3067	–0.3396
PC3	–0.6173	–0.6480	–0.0560	0.4162	0.1339	0.0680	0.0111

Note: PC1, PC2, and PC3 are the first, second, and third principal components, respectively; TCT is the tasseled cap transformation wetness component.

This should also prove true in a temporal context, since visible and SWIR are far more sensitive to water loss than NIR (Carter 1991).

A surprising result is found with ASTER PC3, where the correlation with SMC ($r^2 = 0.490$) is nearly as strong as that of PC2 ($r^2 = 0.517$). Covariance analysis, however, indicates that the PC3 accounts for less than 3% of the spectral variation (data not shown). The high correlation may be due to the fact that PC3 eigenvector coefficients are positive only in the SWIR (Table 4B), and so the water-absorption bands are contrasted with bands that are not water absorptive.

Sources of error

There were several possible sources of error in the study. First, plots were rarely contained entirely within one pixel, and because the georegistration of the images produced an RMSE = 0.7 pixel, the pixel chosen for analysis may not necessarily be the most accurate representation of the plot. Determining the spatial autocorrelation of SMC at the scale of one or two pixels would in theory be helpful for quantifying this potential geolocation error, but the type of sampling required to quantify SMC autocorrelation at such a fine scale was beyond the scope of this study. Second, Ω_E values were unrealistically high at some plots with sparse canopies, generating inflated SMC values. Third, satellites are more apt to detect light reflected by the upper canopy rather than the lower canopy, where FMC is typically higher. Therefore, tall, mature stands with high degrees of canopy closure would reflect more SWIR than would shorter stands of equal SMC.

When evaluating ecosystem monitoring potential, spatial variability of SMC served as a proxy for temporal variability in this study. This analog may not offer the same physical and spectral disparities as may be observed through time. Nonetheless, this surrogate can be instructive and appears elsewhere in the literature (e.g., Serrano et al. 2000). The SWIR region demonstrates high sensitivity to curing for a given leaf of constant mass and structure (Fig. 1). A hypothetical plot experiencing moisture stress would not necessarily exhibit the same spectral signature as a sparser plot of equal SMC with healthy, moist leaves. The biomass variable becomes salient here: the former plot would likely exhibit slightly higher NIR reflectance than the latter plot. Different results might be found in a similar study where plots are monitored remotely and moisture is measured repeatedly in the field. It might be advantageous to use MI1–3 in such a case, where the loss of chlorophyll and corresponding increase in red reflectance would amplify the contrast with NIR reflectance.

Applications for forest monitoring

Regular monitoring of vegetation in the United States is practiced by the US Forest Service via "departure from average NDVI" (Burgan et al. 1996):

$$[11] \quad DA = \frac{NDVI}{NDVI_A} \times 100\%$$

where DA is departure from average, NDVI is the current value, and $NDVI_A$ is the average NDVI for that time period, as averaged over a 5-year period (1989–1994) from Advanced Very High Resolution Radiometer (AVHRR) data. NDVI, however, only responds to the secondary effects of vegetation senescence (chlorophyll loss and shrinking of leaf cells). Moisture and chlorophyll concentrations, however, are not inextricably correlated and may vary individually due to a number of internal and environmental forcings (Larcher 1995). Ceccato et al. (2001) provide a thorough examination of such a monitoring method, and citing several examples in the literature of the decoupling of moisture variation and chlorophyll concentration, they conclude that the DA method is inadequate.

Our analysis shows that NDVI demonstrates relatively little sensitivity to SMC ($r^2 = 0.376$). Strong coupling of SWIR reflectance and water content makes the tested methods more applicable to regional- and continental-scale monitoring of vegetation. The wNDII or TCT wetness can be substituted for NDVI to yield higher accuracy in environmental stress and fire-potential diagnosis. In addition, it is suggested that the index should also factor in seasonal maximum values to account for annual variations in understory vegetation (potential fuels). The fuller the understory growth during the spring flush, the more understory fire fuels can be expected later in the season. One proposed form is

$$[12] \quad DA_{NDII} = \frac{wNDII\,[1 - (wNDII_{MAX} - wNDII)]}{wNDII_A} \times 100\%$$

where wNDII is the current index value, $wNDII_{MAX}$ is the seasonal maximum, and $wNDII_A$ is the average value for the given time period. By contrasting the current and seasonal

maximum wNDII values, the proposed index is able to account for the curing of the annually variable ground cover as well as the departure from the average. Prior to full spring flush for a site, the index could only be employed without the parenthetical component. This is of little consequence to most North American regions, where the principal fire season occurs during the mid- to late- summer dry periods, underscoring the potential utility of such an approach.

Conclusions

The potential of five different SWIR-derived indices, PCA, and TCT wetness for estimating SMC in an ecosystem dominated by *P. ponderosa* has been determined. Fifty-one plots were established within and near the Black Hills Experimental Forest in the Black Hills of South Dakota, and the ground data were compared with Landsat and ASTER imagery. Among the indices, NDII exhibited the strongest correlation with ground data. The NDII relationship was strengthened by a twofold weighting of the NIR channel, creating a weighted NDII (wNDII). The TCT wetness component performed similarly to wNDII. Sixteen plots were excluded from analysis for either of two reasons: (1) they were characterized by dense understories of broadleaved grasses or (2) there was an extended lapse between field and satellite acquisition. With this refined data set, the r^2 of wNDII to SMC increased from 0.627 to 0.834.

PCA was applied to the 5 August 2003 Landsat image and the 21 July 2003 ASTER image to determine correlations with foliar water. Landsat's PC2 exhibited a strong, positive correlation ($r^2 = 0.765$) with SMC. The strong performance of the PCA suggests potential for use in conjunction with hyperspectral remote sensing. Of the several published studies on hyperspectral remote sensing of landscape-level foliar moisture, none have used PCA (e.g., Roberts et al. 1997; Ustin et al. 1998; Serrano et al. 2000). This powerful data-reduction tool, though, may serve as an indicator of SMC. Since PCA is data dependent, it is functional only for single-date analyses of foliar moisture and cannot be used for quantitative monitoring of forests. Consequently, for applications that require periodic analysis and comparison, calculating the weighted NDII or TCT wetness component with multispectral sensors is the most suitable approach for estimating SMC (the latter method may only be implemented with Landsat at this time).

ASTER performed more poorly than Landsat with the aforementioned approaches (excluding the TCT and MI3, which are not possible at this time with ASTER). The slight advantage of band 4 suggests that cross-talk, while it primarily affects bands 5 and 9, may be contaminating the entire SWIR spectrum. Landsat TM is an aged sensor with less than optimal signal to noise ratios. Nevertheless, it appears that the older sensor may be superior to ASTER for remote sensing foliar moisture using the SWIR indices and image transformation.

A modification was made to the "departure from average NDVI" (Burgan et al. 1996) method of forecasting fire potential to increase the sensitivity to primary effects of curing and annual variations in ground cover. Incorporation of wNDII and annual maximum vegetation cover should yield more accurate assessments of fire susceptibility in forested ecosystems. Such monitoring may be performed with several satellites that detect SWIR radiance with high spatial resolution (Landsat 5/7, ASTER, Système pour l'Observation de la Terre (SPOT)) and temporal (MODIS) resolution.

A majority of the research using SWIR for estimating foliar moisture has been conducted in mid- and high-latitude sites. Though SWIR has been used for remote sensing studies in the humid tropics (e.g., Steininger 1996), further study to determine the effect of high water vapor content on biophysical parameter estimates is warranted. In addition, using multispectral sensors in combination with physically based EWT derivation calculated through leaf and canopy reflectance models may improve remote derivation of SMC.

Acknowledgements

This research was funded by NASA EPSCoR grant NCC5-588; L. Vierling, PI. Thanks are given to Patrick Zimmerman, Kerri Vierling, Maribeth Price, Alistair Smith, Connie Crandall, and two anonymous reviewers for their useful comments on the original manuscript. We are very grateful for the assistance in the field provided by Bruce Hoon, Meghan Calhoon, Shane Hansen, and Eric Rowell.

References

Al-Abbas, A.H., Barr, R., Hall, J.D., Crane, F.L., and Baumgardner, M.F. 1974. Spectra of normal and nutrient-deficient maize leaves. Agronomy, **66**: 16–20.

Birth, G.S., and McVey, G. 1968. Measuring the color of growing turf with a reflectance spectrophotometer. Agronomy, **60**: 640–643.

Burgan, R.E., Hartford, R.A., and Eidenshink, J.C. 1996. Using NDVI to assess departure from average greenness and its relation to fire business. USDA For. Serv. Gen. Tech. Rep. INT-GTR-73.

Carter, G.A. 1991. Primary and secondary effects of water content on the spectral reflectance of leaves. Am. J. Bot. **78**(7): 916–924.

Ceccato, P., Flasse, S., Tarantola, S., Jacquemoud, S., and Gregoire, J.M. 2001. Detecting vegetation in leaf water content using reflectance in the optical domain. Remote Sens. Environ. **77**: 22–33.

Ceccato, P., Gobron, N., Flasse, S., Pinty, B., and Tarantola, S. 2002*a*. Designing a spectral index to estimate vegetation water content from remote sensing data. Part 1. Theoretical approach. Remote Sens. Environ. **82**: 188–197.

Ceccato, P., Flasse, S., and Gregoire, J.M. 2002*b*. Designing a spectral index to estimate vegetation water content from remote sensing data. Part 2. Validation and applications. Remote Sens. Environ. **82**: 198–207.

Chavez, P.S. 1988. An improved dark-object subtraction technique for atmospheric scattering correction of multispectral data. Remote Sens. Environ. **24**: 459–479.

Chen, J.M. 1996. Optically-based methods for measuring seasonal variation of leaf area index in boreal conifer stands. Agric. For. Meteorol. **80**: 135–163.

Chen, J.M., Pavlic, G., Brown, L., Cihlar, J., Leblanc, S.G., White, S.G. et al. 2002. Derivation and validation of Canada-wide coarse-resolution leaf area index maps using high-resolution satellite imagery and ground measurements. Remote Sens. Environ. **80**: 165–184.

Chuvieco, E., Vaughan, P., Riaño, D., and Cocero, D. 1999. Fire danger and fuel moisture content estimation from remotely

sensed data. *In* Crossing the Millennium: Integrating Spatial Technologies and Ecological Principles for a New Age in Fire Management. Proceedings from the Joint Fire Science Conference and Workshop, Boise, Idaho, 15–17 June 1999. *Technical editing by* L.F. Neuenschwander and K.C. Ryan. University of Idaho, Moscow, Idaho. [Abstr.]

Collins, J.B., and Woodcock, C.E. 1996. An assessment of several linear change detection techniques for mapping forest mortality using multitemporal Landsat TM data. Remote Sens. Environ. **56**: 66–77.

Crist, E.P., Laurin, R., and Cicone, R.C. 1986. Vegetation and soils information contained in transformed Thematic Mapper data. *In* Proceedings of IGARSS' 1986 Symposium, Zurich, Switzerland, 8–11 September 1986. pp. 1465–1470.

Dawson, T.P., Curran, P.J., North, P.R.J., and Plummer, S.E. 1999. The propagation of foliar biochemical absorption features in forest canopy reflectance: a theoretical analysis. Remote Sens. Environ. **67**: 147–159.

Dennison, P.E., Roberts, D.A., Thorgusen, S.R., Rugelbrugge, J.C., Weise, D., and Lee, C. 2003. Modeling seasonal changes in live fuel moisture and equivalent water thickness using a cumulative water balance index. Remote Sens. Environ. **88**: 442–452.

Dennison, P.E., Roberts, D.A., Peterson, S.H., and Rechel, J. 2004. Use of normalized difference water index for monitoring live fuel moisture. Int. J. Remote Sens. **26**(5): 1035–1042.

Earth Remote Sensing Data Analysis Center. 2002. Release notes: What is crosstalk [online]? Available from http://www.gds.aster.ersdac.or.jp/gds_www2002/service_e/release_e/set_release_ecrs.html [cited 14 April 2004].

Gao, B.C. 1996. NDWI — A normalized difference water index for remote sensing of vegetation liquid water from space. Remote Sens. Environ. **58**: 257–266.

Gao, X., Huete, A.R., Ni, W., and Miura, T. 2000. Optical–biophysical relationships of vegetation spectra without background contamination. Remote Sens. Environ. **74**: 609–620.

Gates, D.M., Keegan, H.J., Schleter, J.C., and Weidner, V.R. 1965. Spectral properties of plants. Appl. Optics, **4**(1): 11–20.

Gausman, H.W., Allen, W.A., Wiegand, C.L., Escobar, D.E., Rodriguez, R.R., and Richardson, A.J. 1973. The leaf mesophylls of twenty crops, their light spectra, and optical and geometrical parameters. USDA Agric. Res. Serv. Tech. Bull. 1465.

Hall, F.G., Shimabukuro, Y.E., and Huemmrich, K.F. 1995. Remote sensing of forest biophysical structure using mixture decomposition and geometric reflectance models. Ecol. Appl. **5**(4): 993–1013.

Hardisky, M.A., Smart, R.M., and Klemas, V. 1983. Seasonal spectral characteristics and aboveground biomass of the tidal marsh plant, *Spartina alterniflora*. Photogramm. Eng. Remote Sens. **49**(1): 85–92.

Hardy, C.C., and Burgan, R.E. 1999. Evaluation of NDVI for monitoring live moisture in three vegetation types of the western US. Photogramm. Eng. Remote Sens. **65**(5): 603–610.

Huete, A.R., Liu, H.Q., Batchily, K., and van Leeuwen, W. 1997. A comparison of vegetation indices over a global set of TM images for EOS-MODIS. Remote Sens. Environ. **59**: 440–451.

Huete, A., Didan, K., Miura, T., Rodriguez, E.P., Gao, X., and Ferreira, L.G. 2002. Overview of the radiometric and biophysical performance of the MODIS vegetation indices. Remote Sens. Environ. **83**: 195–213.

Jacquemoud, S., Baret, F., Andrieu, B., Danson, F.M., and Jaggard, K. 1995. Extraction of vegetation biophysical parameters by inversion of the PROSPECT + SAIL models on sugar beet canopy reflectance data. Application to TM and AVIRIS sensors. Remote Sens. Environ. **52**: 163–172.

Larcher, W. 1995. Physiological plant ecology: ecophysiology and stress physiology groups. 3rd ed. Springer-Verlag, New York.

Law, B.E., Van Tuyl, S., Cescatti, A., and Baldocchi, D.D. 2001. Estimation of leaf area index in open canopy ponderosa pine forests at different successional stages and management regimes in Oregon. Agric. For. Meteorol. **108**: 1–14.

Lillesaeter, O. 1982. Spectral reflectance of partly transmitting leaves: laboratory measurements and mathematical modeling. Remote Sens. Environ. **12**: 247–254.

Maki, M., Ishiahra, M., and Tamura, M. 2004. Estimation of leaf water status to monitor the risk of forest fires by using remotely sensed data. Remote Sens. Environ. **90**: 441–450.

Miura, T., Huete, A.R., Yoshioka, H., and Holben, B.N. 2001. An error and sensitivity analysis of atmospheric resistant vegetation indices derived from dark target-based atmospheric correction. Remote Sens. Environ. **78**: 284–298.

Peñuelas, J., Filella, I., Biel, C., Serrano, L., and Savé, R. 1993. The reflectance at the 950–970 nm region as an indicator of plant water status. Int. J. Remote Sens. **14**(10): 1887–1905.

Roberts, D.A., Green, R.O., and Adams, J.B. 1997. Temporal and spatial patterns in vegetation and atmospheric properties from AVIRIS. Remote Sens. Environ. **62**: 223–240.

Roberts, D.A., Ustin, S.M., Ogunjemiyo, S., Greenberg, J., Dobrowski, S.Z., Chen, J., and Hinckley, T.M. 2004. Spectral and structural measurements of Northwest forest vegetation at leaf to landscape levels. Ecosystems, **7**(5): 545–562.

Rouse, J.W., Haas, R.H., Schell, J.A., and Deering, D.W. 1974. Monitoring vegetation systems in the Great Plains with ERTS. *In* Proceedings of the Third Earth Resource Technology Satellite-1 Symposium, Greenbelt, Md. NASA, SP-351. pp. 3010–3017.

Schowengerdt, R.A. 1997. Principal components. *In* Remote sensing: models and methods for image processing. 2nd ed. Academic Press, San Diego. pp. 187–198.

Sellers, P.J. 1985. Canopy reflectance, photosynthesis, and transpiration. Int. J. Remote Sens. **6**(8): 1335–1372.

Serrano, L., Ustin, S.L., Roberts, D.A., Gamon, J.A., and Penuelas, J. 2000. Deriving water content of chaparral vegetation from AVIRIS data. Remote Sens. Environ. **74**: 570–581.

Sims, D.A., and Gamon, J.A. 2003. Estimation of vegetation water content and photosynthetic tissue area from spectral reflectance: a comparison and indices based on liquid water and chlorophyll absorption features. Remote Sens. Environ. **84**: 526–537.

Skakun, R.S., Wulder, M.A., and Franklin, S.E. 2003. Sensitivity of the thematic mapper enhanced wetness difference index to detect mountain pine beetle red-attack damage. Remote Sens. Environ. **86**: 433–443.

Spanner, M., Johnson, L., Miller, J., McCreight, R., Freemantle, J., Runyon, J., and Gong, P. 1994. Remote sensing of seasonal leaf area index across the Oregon Transect. Ecol. Appl. **4**(2): 258–271.

Spanner, M.A., Pierce, L.L., Peterson, D.L., and Running, S.W. 1990. Remote sensing of temperate coniferous forest leaf area index. The influence of canopy closure, understorey vegetation and background reflectance. Int. J. Remote Sens. **11**(1): 95–111.

Steininger, M.K. 1996. Tropical secondary forest regrowth in the Amazon: age, area and change estimation with Thematic Mapper data. Int. J. Remote Sens. **17**(1): 9–27.

Stimson, H.C., Breshear, D.D., Kefauver, S.C., and Ustin, S.L. 2003. Spectral sensing of foliar water conditions in two conifer species. *In* Proceedings of the 88th Annual Ecological Society of America Meeting, Savannah, Ga., 3–8 August 2003.

Stow, D., Kaiser, J., Niphadkar, M., Gantcheva, E., and Coulter, L. 2004. Monitoring changes in fuel moisture conditions of south-

ern California chaparral based on time series of MODIS-derived indices. *In* Proceedings of the 2004 ASPRS Annual Conference, Denver, Colo., 24–28 May 2004.

Thome, K., Biggar, S., and Takashima, T. 1999. Algorithm Theoretical Basis Document for ASTER Level 2B-1 and ASTER Level 2B5. Remote Sensing Group of the Optical Sciences Center, University of Arizona, Tuscon.

Tucker, C.J. 1980. Remote sensing of leaf water content in the near infrared. Remote Sens. Environ. **10**: 23–32.

USGS. 2003. Real time data for South Dakota: precipitation [online]. Available from http://waterdata.usgs.gov/sd/nwis/current?type=precip&group_key=basin_cd [cited 14 November 2003].

Ustin, S.L., Roberts, D.A., Pinzon, J., Jacquemond, S., Gardner, M., Scheer, G., Castaneda, C.M., and Palacios-Orueta, A. 1998. Estimating canopy water content of chaparral shrubs using optical methods. Remote Sens. Environ. **65**: 280–291.

Wessman, C.A., Aber, J.D., Peterson, D.L., and Mellilo, J.M. 1988. Remote sensing of canopy chemistry and nitrogen cycling in temperate forest ecosystems. Nature (London), **335**: 154–156.

Woolley, J.T. 1971. Reflectance and transmittance of light by leaves. Plant Physiol. **47**: 656–662.

Wulder, M.A., LeDrew, E.F., Franklin, S.E., and Lavigne, M.B. 1998. Aerial image texture information in the estimation of northern deciduous and mixed wood forest leaf area index. Remote Sens. Environ. **64**: 64–76.